

# TIDAL: Temporally Interleaved Diffusion and Action Loop for High-Frequency VLA Control

Yuteng Sun<sup>1,2</sup>, Haoran Wang<sup>1,3</sup>, Ruofei Bai<sup>1,3</sup>, Zhengguo Li<sup>1</sup>, Jun Li<sup>1</sup>,  
Meng Yee (Michael) Chuah<sup>1</sup> and Wei Yun Yau<sup>1</sup>

<sup>1</sup>Institute for Infocomm Research (I<sup>2</sup>R), A\*STAR, Singapore

<sup>2</sup>Tsinghua University, Beijing, China

<sup>3</sup>Nanyang Technological University, Singapore

**Abstract**—Large-scale Vision-Language-Action (VLA) models offer semantic generalization but suffer from high inference latency, limiting them to low-frequency batch-and-execute paradigm. This frequency mismatch creates an execution blind spot, causing failures in dynamic environments where targets move during the open-loop execution window. We propose TIDAL (Temporally Interleaved Diffusion and Action Loop), a hierarchical framework that decouples semantic reasoning from high-frequency actuation. TIDAL operates as a backbone-agnostic module for diffusion-based VLAs, using a dual-frequency architecture to redistribute the computational budget. Specifically, a low-frequency macro-intent loop caches semantic embeddings, while a high-frequency micro-control loop interleaves single-step flow integration with execution. This design enables approximately 9 Hz control updates on edge hardware (vs. approximately 2.4 Hz baselines) without increasing marginal overhead. To handle the resulting latency shift, we introduce a temporally misaligned training strategy where the policy learns predictive compensation using stale semantic intent alongside real-time proprioception. Additionally, we address the insensitivity of static vision encoders to velocity by incorporating a differential motion predictor. TIDAL is architectural, making it orthogonal to system-level optimizations. Experiments show a 2x performance gain over open-loop baselines in dynamic interception tasks. Despite a marginal regression in static success rates, our approach yields a 4x increase in feedback frequency and extends the effective horizon of semantic embeddings beyond the native action chunk size. Under non-paused inference protocols, TIDAL remains robust where standard baselines fail due to latency.

**Index Terms**—Vision-Language-Action Models, Flow Matching, Dynamic Manipulation

## I. INTRODUCTION

The pursuit of generalist embodied agents has been accelerated by Vision-Language-Action models, exemplified by systems like GR00T [1] and  $\pi_0$  [2]. These state-of-the-art models increasingly adopt hierarchical architectures that integrate large Vision-Language-Model backbones with continuous diffusion or flow-matching heads. While these models offer strong semantic grounding by internet-scale pre-training, their architectural scale creates a severe computational bottleneck. Current VLAs typically operate on a batch-and-execute paradigm: the system pauses to process observations and computes an entire long-horizon action chunk, which is then executed open-loop. This introduces a fundamental frequency mismatch. Dynamic manipulation requires high-frequency control, yet large-scale VLM inference is often bound

to 2–5 Hz [3], [4]. In real-world deployment, this bottleneck is worsened by the mandatory execution time of the generated action chunk [5], [6]. The combination of inference latency and open-loop execution creates an execution blind spot, where the robot remains unresponsive to environmental changes, leading to failures in dynamic interception tasks.

Existing latency mitigation strategies incur significant trade-offs. System-level optimizations, such as quantization (e.g., BitVLA [7]) or token pruning (e.g., FlashVLA [8]), provide speedups but remain bounded by the sequential attention mechanism. Distilling small-scale policies like TinyVLA [9] trades rich semantic priors for throughput. More recently, asynchronous scheduling [5] and dual-system architectures [10], [11] have attempted to decouple execution from reasoning. However, these methods often require complex stream management or separate policy networks. We argue that high-frequency control should not require losing the semantic intelligence of large foundation models, nor should it require training distinct policies.

We propose TIDAL (Temporally Interleaved Diffusion and Action Loop), a backbone-agnostic framework that bridges this frequency gap via compute-efficient interleaved scheduling. Our core insight is that semantic intent exhibits high temporal persistence, whereas physical state is highly transient. Consequently, the expensive VLM backbone need not be queried synchronously at every step. Instead of discarding the semantic context, we extend its lifespan by fusing it with high-frequency, real-time proprioceptive updates. TIDAL employs a hierarchical dual-frequency Architecture: a low-frequency macro-loop caches semantic embeddings, while a high-frequency micro-loop interleaves single-step flow integration with execution. By algorithmically compressing action chunk generation to negligible levels via single-step flow integration, we achieve the responsiveness of parallel systems without their hardware cost. This redistributes the computational budget, refreshing the action chunk every  $\sim$ 110 ms ( $\approx$  9 Hz) compared to the standard  $\sim$ 400 ms baseline cycle, yielding a 4 $\times$  increase in feedback frequency. Although this imposes a higher optimization burden that slightly impacts static task convergence, it provides the critical reactivity required for dynamic interaction and extends the lifespan of semantic embeddings beyond the native action chunk size.



Fig. 1. *Dynamic Interception Task Execution*. A complete rollout where TIDAL (1) intercepts a moving can, (2) places it into the drawer, and (3) closes the drawer. Unlike open-loop baselines, TIDAL’s high-frequency micro-control loop enables the robot to reactively track the moving target and robustly complete the long-horizon sequence.

Deploying this decoupled architecture introduces a temporal misalignment between the stale semantic condition and the current physical state. To address this, we introduce a temporally misaligned training strategy where the policy learns predictive compensation, using current proprioception to correct for outdated visual intent. Additionally, we resolve the velocity insensitivity of static vision encoders by incorporating a Differential Motion Predictor with contact-gated injection.

Our primary contributions are:

- 1) A dual-loop framework that densifies the control updates of heavy VLA backbones by decoupling intent generation from actuation.
- 2) A training paradigm that enables the policy to robustly compensate for variable VLM latencies and stale semantic cues.
- 3) An optimized flow matching inference strategy leveraging source-biased sampling training to compress action chunk generation into a single execution step, facilitating high-frequency interleaving.
- 4) TIDAL achieves a  $2\times$  performance gain in dynamic interception tasks and maintains robustness under non-paused inference evaluation.

## II. RELATED WORK

### A. Evolution of VLA: Towards Hierarchical Flow

Early VLM-as-a-policy approaches, such as RT-2 [12] and OpenVLA [13], adopt a VLM + discrete action token architecture. They map natural language directly to quantized actions via large-scale pre-training. To enable continuous control, recent works moved to diffusion and flow matching policies. Models like Octo [14] and  $\pi_0$  [2] replace discrete heads with diffusion processes [15] or flow matching experts.

More recently, hierarchical architectures have become standard. Systems like GR0OT [1] and  $\pi_0.5$  [16] combine a heavy VLM backbone for reasoning with a separate Diffusion Transformer (DiT) for action generation. Despite this decoupling, the main inference strategy remains the batch-and-execute paradigm. Even hierarchical systems typically query the VLM and action head synchronously at the start of a cycle. The computational cost of the VLM limits the control frequency to 2–5 Hz [3]. This creates an execution blind spot: a window where high-frequency motor control freezes or runs open-loop while waiting for the next update. TIDAL targets this specific inefficiency in hierarchical flow-based architectures.

### B. Latency Mitigation and Real-Time Inference

Current methods bridge the inference-actuation gap through model simplification, adaptive computation, or parallel scheduling.

1) *Model Distillation and Architectural Simplification*: One strategy is to train smaller policies or replace heavy Transformer backbones. Mobile ALOHA [17] and TinyVLA [9] show that compact models achieve high throughput. SmoVLA [18] uses parameter-efficient fine-tuning on consumer hardware and RoboMamba [19] uses state-space models to reduce complexity. These methods gain speed by losing the rich semantic priors and reasoning of large foundation models. Consistency Policy [20] accelerates inference by distilling diffusion heads into single-step solvers. This only addresses action head latency, leaving the VLM backbone bottleneck unresolved. TIDAL retains the full backbone, achieving small-model speed without losing large-model intelligence.

2) *Static Compression and Adaptive Inference*: Many works optimize the backbone directly. Static techniques like quantization (e.g., BitVLA [7], AWQ [21]) and token pruning (e.g., FlashVLA [8], EfficientVLA [22]) reduce memory and compute density. Dynamic inference mechanisms such as DeeR-VLA [23] and CEED-VLA [24] use early exit strategies to stop the forward pass when confidence is high. MoLe-VLA [25] optimizes compute via dynamic layer routing, while EdgeVLA [26] and PD-VLA [27] remove autoregressive dependencies via parallel decoding or specialized heads. System-level optimizations [28] also enable real-time throughput via kernel fusion. Although these methods reduce computation per step, they remain bound by the sequential observe-then-act bottleneck. TIDAL is orthogonal to these optimizations; it acts as a temporal scheduler that uses these accelerated backbones to further densify replanning cycles.

3) *Asynchronous Pipeline and Future Awareness*: Recent works optimize the inference pipeline via asynchronous execution to break sequential dependencies. Real-Time Chunking [5] inpaints future actions during execution, while VLASH [6] uses a future-state-aware paradigm. VLASH trains the policy to compensate for latency by conditioning on predicted future states. Similarly, Spec-VLA [29] accelerates decoding via speculative sampling. TIDAL shares the insight of training with temporal misalignment but diverges in execution. Pipelined approaches require high VLM throughput to minimize the prediction horizon. In contrast, TIDAL’s lightweight micro-loop reduces effective calculation time to minimal levels. This allows TIDAL to condition directly on the current fused state,

avoiding the complexity and uncertainty of predicting future system states.

4) *Decoupled and Dual-System Architectures*: A recent paradigm decouples semantic reasoning from motor control into separate processes. Concurrent frameworks like DuoCore-FS [30] and Fast-in-Slow [10] implement a parallel architecture: a slow VLM updates a latent buffer in the background, while a fast policy queries this buffer at high frequency. Although this enables asynchronous execution, it imposes a heavy hardware burden, requiring sufficient memory bandwidth and compute to sustain two active models simultaneously. TIDAL achieves similar decoupling via an *Interleaved* rather than Parallel strategy. By treating the VLM and Action Head as serial but temporally multiplexed components, TIDAL maximizes compute utilization on edge devices. Unlike DuoCore-FS, which relies on hardware parallelism, TIDAL uses a single-step flow integration mechanism. This algorithmically compresses micro-loop latency, ensuring high-frequency reactivity within a serial execution budget. We validate this responsiveness through dynamic simulation benchmarks, providing quantitative analysis of interception performance under realistic non-paused inference constraints.

### C. Temporal Redundancy and Action Generation

Recent works on VLA efficiency [31] leverage the insight that physical states change rapidly, but high-level semantic intent persists. This insight drives techniques like VLA-Cache [32], which reuses attention KV-caches for static patches, and Fast ECoT [33], which caches high-level language plans. TIDAL extends this philosophy from feature-level to semantic embedding level. We freeze the heavy semantic embedding while querying the lightweight flow policy, exploiting the redundancy in the task intention.

### D. Action Chunking and Execution Strategies

Action chunking [34] is the standard execution paradigm for VLA models like OpenVLA [13] and A0 [35]. Predicting a fixed-horizon action chunk distributes the computational cost of the backbone. But the prevailing execution strategy remains open-loop, the robot executes the chunk blindly while the planner freezes for the next cycle. This causes temporal discontinuities at chunk boundaries and makes the system unresponsive to dynamic disturbances during the long execution window.

Recent efforts reduce these artifacts through advanced scheduling. Real-Time Chunking (RTC) [5] treats asynchronous execution as inference-time inpainting, generating the next chunk while executing the previous one. Training-Time Action Conditioning (TTAC) [36] optimizes this by simulating latency to condition on executing prefixes. Bidirectional Decoding [37] uses rejection sampling to splice chunks. Although these asynchronous methods improve throughput, they fundamentally condition actions on stale observations captured at the start of the inference delay.

TIDAL moves away from this predict-then-execute. Leveraging the vector field properties of Flow Matching [38], we

treat the action chunk not as a rigid chunk, but as a flexible manifold. Our *Interleaved Single-Step Integration* injects the latest proprioceptive state into the solver at every step. This transforms the chunk from a static plan into a dynamic vector field query, enabling high frequency reactivity without the complexity of asynchronous stream management or the latency of full sequence regeneration.

## III. METHODOLOGY

### A. Hierarchical Dual-Frequency Architecture

TIDAL splits VLA inference into two nested processes: a low-frequency macro-intent loop for semantic reasoning and a high-frequency micro-control loop for closed-loop refinement. This decomposition allows 3B parameter backbones to run at high control frequencies by caching semantic embeddings and interleaving flow matching integration steps.

1) *Macro-Intent Loop (Semantic Caching)*: The macro loop extracts high-level intent from visual observations. Let  $l_{\text{instr}}$  denote the natural language instruction and  $I_{t_k}$  denote the RGB observation at macro-step  $k$ . We use a pre-trained VLM backbone  $\Phi_{\text{VLM}}$  to map these inputs to a dense intent embedding  $\mathcal{E}_k$ :

$$\mathcal{E}_k = \Phi_{\text{VLM}}(I_{t_k}, l_{\text{instr}}) \quad (1)$$

The embedding  $\mathcal{E}_k$  is stored in a latent intent and remains frozen for the macro-cycle (horizon  $H = 16$ ). This caching strategy isolates the control loop from the high latency of  $\Phi_{\text{VLM}}$ , exploiting the fact that semantic intent persists over short execution horizons.

2) *Micro-Control Loop (Interleaved Flow Execution)*: The micro loop functions as a stateless policy that queries the action head at high frequency. To align with the standard execution horizon ( $H = 16$ ) while maximizing feedback density, we structure the inference as a cascade of  $K = 4$  interactions per macro-cycle. Given a cached intent  $\mathcal{E}$ , the loop iterates through latency stages  $k \in \{0, \dots, K-1\}$ . At each stage, it observes the current fused state  $\tilde{s}_{k:N}$  and performs a single-step Euler integration to generate the action chunk  $\hat{a}$ :

$$\hat{a} = x_0 + v_\theta(x_0, 0, \tilde{s}_{k:N}, \mathcal{E}) \quad (2)$$

where  $x_0 \sim \mathcal{N}(0, I)$  represents the source noise at flow time  $t = 0$ , and  $v_\theta$  predicts the vector field pointing towards the data manifold. After chunk generation, we execute only the first  $N$  steps ( $\hat{a}[0:N]$ ) on the robot hardware, discarding the rest.

Standard baselines exhaust the entire integration budget (e.g.,  $K = 4$  solver steps) at  $t = 0$ . In contrast, TIDAL distributes this budget across the timeline. Building on streaming execution paradigms [39], [40], we use a single integration step, which yields a sufficiently accurate vector direction for closed-loop stability. By executing a single Euler step—effectively a local flow update—at every chunk boundary, we maintain a Backbone-Iso-Compute footprint while increasing the action chunk update frequency by  $4\times$ . While standard baselines suffer from a long update cycle ( $\sim 400$  ms), TIDAL reduces this local control cycle to  $\sim 100$  ms. This acts as a local vector field

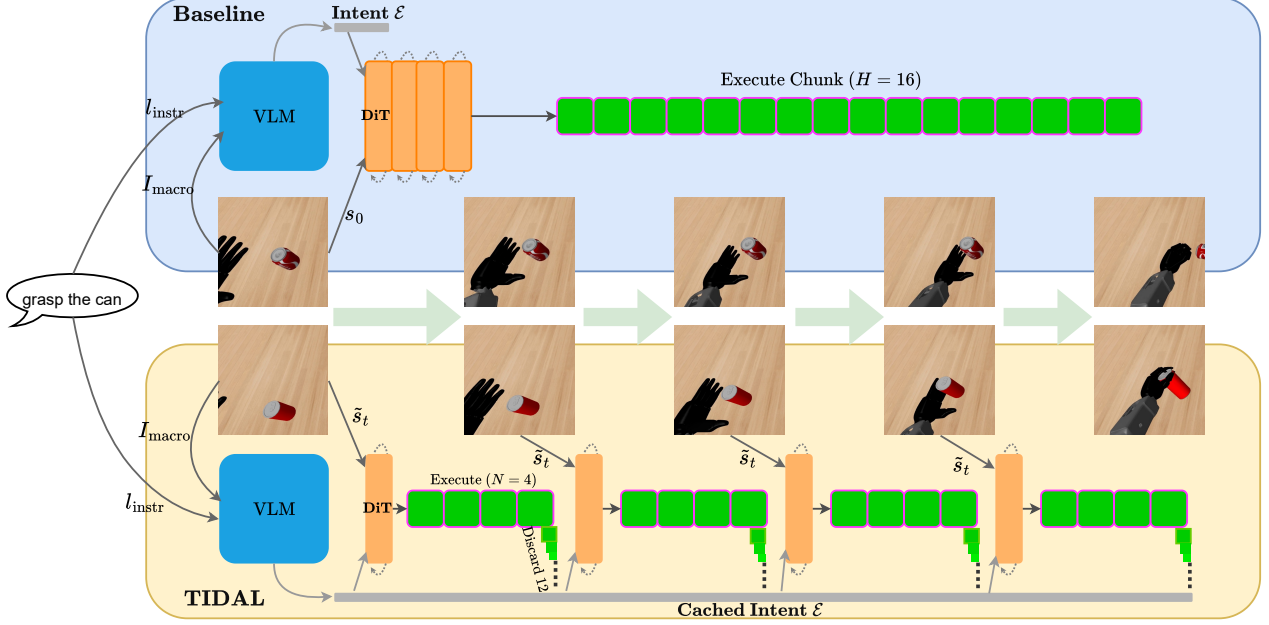


Fig. 2. Comparison of Inference Paradigms in Dynamic Interception. (Top) *Standard Baseline*: Under the batch-and-execute model, the system performs a blocking inference at the start. It generates a fixed 16-step action chunk conditioned on the static initial state  $s_0$ . The resulting open-loop execution forces the robot to follow a stale trajectory, missing the moving target. (Bottom) *TIDAL (Ours)*: Our Hierarchical Dual-Frequency Architecture. The macro-loop queries the VLM once to generate a Cached Intent  $\mathcal{E}$  (grey bar), decoupling expensive reasoning from high-frequency actuation. The micro-loop performs interleaved flow integration. At each update, the DiT combines the frozen intent with the real-time fused state  $\tilde{s}_t$  to generate a fresh trajectory. The policy executes only the immediate chunk ( $N = 4$ ) and discards the tail (fading blocks). This sliding-window execution refreshes the control signal at  $\sim 9$  Hz, enabling the robot to robustly intercept dynamic objects.

query, correcting action chunk drift via updated  $s_{t_i}$  rather than expensive long-horizon replanning.

### B. Temporally Misaligned Training

Synchronous training creates a distribution shift in our architecture because semantic conditions  $\mathcal{E}$  ( $I_{t-\Delta}$ ) lag behind the physical state  $s_t$ . We address this with a temporally misaligned training strategy that explicitly decouples visual and physical input timestamps. This aligns with recent findings in asynchronous control [6], [30], confirming that conditioning policies on latency-matched proprioception enables convergence despite semantic lag.

1) *Dynamic Latency Injection*: We simulate variable inference latencies by creating training samples with randomized time-lags. Instead of fixed windows  $H$ , we sample extended trajectory segments of length  $L$ :

$$L = H + (K - 1) \times N \quad (3)$$

where  $H = 16$  is the prediction horizon,  $N = 4$  is the execution chunk size, and  $K = 4$  is the number of latency stages. We set  $L = 28$ .

During training, we discretize the potential delay into fixed stages, sampling a latency index  $k \sim \mathcal{U}\{0, K - 1\}$  for each iteration. The policy input tuple consists of:

- Frozen Intent ( $t = 0$ ): Visual backbone input  $I_0$ .

- Current State ( $t = k \cdot N$ ): Proprioceptive state  $s_{k \cdot N}$ .
- Action Target ( $t = k \cdot N$ ): Ground truth sequence  $a_{k \cdot N:k \cdot N+H}$ .

Restricting latency to a fixed set of discrete multiples of  $N$ , rather than sampling from a continuous interval, reduces the variance of the learning objective. This simplifies the optimization landscape, allowing the model to converge to distinct compensation modes for each stage of intent staleness, rather than fitting an infinite spectrum of delays.

2) *Horizon-Weighted & Time-Biased Flow Matching*: The action chunk generator is implemented using Conditional Flow Matching (CFM) [41], which regresses a time-dependent vector field  $v_\theta$ . We define the optimal transport path  $\psi_t(x_0, x_1) = (1-t)x_0 + tx_1$  between the Gaussian noise source  $x_0 \sim \mathcal{N}(0, I)$  and the target action sequence  $x_1$ . The objective minimizes the expected flow matching error:

$$\mathcal{L}(\theta) = \mathbb{E}_{k, t, x_0, x_1} \left[ \sum_{i=0}^{H-1} w_i \cdot \left\| v_\theta(\psi_t(x_0, x_1), t, s_{k \cdot N}, \mathcal{E}_0)^{(i)} - (x_1^{(i)} - x_0^{(i)}) \right\|^2 \right] \quad (4)$$

---

**Algorithm 1** TIDAL Hierarchical Inference Logic

---

**Require:** VLM Backbone  $\Phi$ , Policy Vector Field  $v_\theta$ , Prediction Horizon  $H = 16$ , Execution Chunk  $N = 4$ , Latency Stages  $K = 4$

- 1: **loop**
- 2:   **{Macro-Intent Loop}**
- 3:   Capture high-res image  $I_{macro}$
- 4:    $\mathcal{E} \leftarrow \Phi(I_{macro}, l_{instr})$  {Blocking Inference ( $\sim 41$  ms), updates intent}
- 5:   **{Micro-Control Loop}**
- 6:   **for**  $k = 0$  **to**  $K - 1$  **do**
- 7:     Capture proprioception  $s_{prop}$  and micro-cam  $I_{micro}$
- 8:      $m_{k:N} \leftarrow \text{MotionPredictor}(I_{micro})$
- 9:      $\tilde{s}_{k:N} \leftarrow \text{Fuse}(s_{prop}, m_{k:N})$  {Dynamic state fusion (Eq. 7)}
- 10:     $x_0 \sim \mathcal{N}(0, I)$  {Sample fresh noise}
- 11:     $\hat{v} \leftarrow v_\theta(x_0, 0, \tilde{s}_{k:N}, \mathcal{E})$  {Inference ( $\sim 19$  ms), condition on  $\tilde{s}_{k:N}$ }
- 12:     $\hat{a}_{raw} \leftarrow x_0 + \hat{v}$  {Generate full trajectory  $H$ }
- 13:    **Execute**  $\hat{a}_{raw}[0:N]$  {Run  $N$  steps, discard tail  $H - N$ }
- 14:    **Wait** for execution ( $\sim 80$  ms @ 50 Hz)
- 15:   **end for**
- 16: **end loop**

---

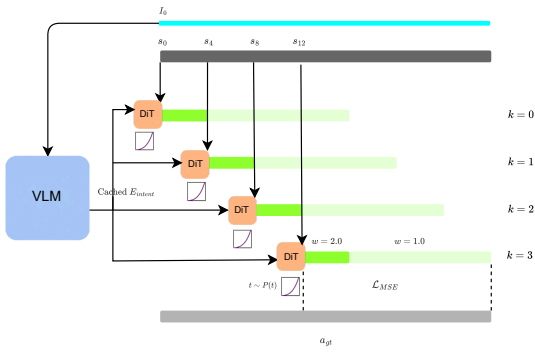


Fig. 3. *Temporally Misaligned Training Strategy*. We decouple the timestamps of visual and physical inputs to handle latency between the macro-Loop and micro-Loop. *Latency Injection (Vertical Axis)*: A single frozen semantic intent (encoded from image  $I_0$ ) is reused across multiple latency stages ( $k = 0, \dots, 3$ ). Training pairs this stale intent with progressively later proprioceptive states ( $s_0, s_4, s_8, s_{12}$ ), enabling the policy to learn predictive compensation for VLM lag. *Optimization Objectives*: We use a Horizon-Weighted Loss (Dark vs. Light Green bars) with weight  $w = 2.0$  for the immediate execution chunk ( $N = 4$ ) to emphasize execution stability. The Time-Biased Sampling inset ( $t \sim P(t)$ ) shows that we bias flow timestep sampling towards the noise source ( $t \approx 0$ ) to optimize the vector field for single-step integration.

where  $t$  is the continuous flow time,  $k \in \{0, 1, 2, 3\}$  represents the sampled latency stage, and  $i$  indexes the action horizon steps.  $s_{k:N}$  and  $\mathcal{E}_0$  denote the time-misaligned proprioception and frozen semantic intent, respectively. The micro-loop executes only the initial chunk of length  $N = 4$  before the next update. So we apply a horizon-aware mask  $w_i$ , setting  $w_i = 2.0$  for

$i < N$  and 1.0 otherwise. This asymmetry forces the vector field to prioritize precision in the imminent execution window ( $i < N$ ) over distal trajectory smoothness.

Standard Flow Matching samples the flow timestep  $t$  uniformly ( $t \sim \mathcal{U}[0, 1]$ ), allocating equal capacity across the probability path. However, our micro-loop relies exclusively on single-step Euler integration starting from pure noise ( $t = 0$ ). The policy is only queried at the source frontier. Training capacity spent minimizing error at intermediate flow times (e.g.,  $t = 0.5$ ) is therefore wasted, as these states are never visited during inference. To align the objective with our architecture, we bias the sampling distribution  $p(t)$  heavily towards the noise source. We sample an auxiliary variable  $s \sim \text{Beta}(\alpha, \beta)$  and set  $t = 1 - s$ . With  $\alpha = 5.0$  and  $\beta = 1.0$ , the probability mass concentrates near  $t \approx 0$ . This ensures the vector field is most accurate exactly where the single-step solver queries it, maximizing the efficiency of the limited inference budget.

### C. Dynamic Perception via Motion Injection

We introduce a Differential Motion Predictor ( $\psi_{\text{motion}}$ ) to inject high-frequency kinematic features directly into the policy, enabling reactivity to moving targets without re-querying the VLM.

We extract motion cues using temporal difference tensors. The input  $\Delta I_t$  is the normalized pixel-wise difference between the current frame and a history frame with lag  $k = 4$ :  $\Delta I_t = \mathcal{T}(I_t) - \mathcal{T}(I_{t-k})$ . A custom 7-layer CNN processes this input to minimize latency, followed by an MLP bottleneck that produces a low-dimensional embedding  $m_t \in \mathbb{R}^{64}$ . We pretrain  $\psi_{\text{motion}}$  using an auxiliary regression loss to predict the end-effector's future position  $p$  and velocity  $v$ , forcing  $m_t$  to encode physical dynamics:

$$\mathcal{L}_{\text{aux}} = \lambda_1 \|\hat{p}_t - p_t\|^2 + \lambda_2 \|\hat{v}_t - v_t\|^2 + \lambda_3 \|\hat{p}_{t+k} - p_{t+k}\|^2 \quad (5)$$

Predicting the future position  $p_{t+k}$  implicitly encodes momentum, enabling predictive interception.

To prevent control instability during manipulation where relative motion is zero, we use a hard contact-gating mechanism. Based on a binary contact state  $c_t \in \{0, 1\}$  derived from gripper sensors, and the robot's proprioceptive joint state  $s_{prop}$ , we construct the fused policy state  $\tilde{s}_t$  via concatenation:

$$\tilde{s}_t = \text{Concat}(s_{prop}, (1 - c_t) \cdot m_t) \quad (6)$$

where  $m_t \in \mathbb{R}^{64}$  is the motion embedding and  $s_{prop}$  is the robot's joint state. This formulation enforces a modal switch: the policy attends to the full motion vector during the approach phase ( $c_t = 0$ ) and receives a zero-masked vector during manipulation ( $c_t = 1$ ), falling back to proprioceptive control upon contact.

## IV. EXPERIMENTS

We evaluate whether TIDAL's hierarchical decoupling enables robust dynamic manipulation without losing generalist capabilities.

### A. Experimental Setup

1) *Environments*: We evaluate TIDAL on two benchmarks in the RoboCasa (MuJoCo) suite:

We use 8 tasks from the official ‘RoboCasa-GR1’ benchmark [1], [42]. These long-horizon tasks feature stationary targets and serve as a control group to verify that our architecture maintains generalist capabilities.

We construct a Dynamic Interception benchmark requiring the robot to intercept a moving target, place it in a drawer, and close it. We initialize the target with a random velocity (0.04–0.06 m/s) along a cardinal direction. To increase stochasticity, the object executes a random 90-degree turn at boundaries, creating non-deterministic trajectories. We stratify this into Easy and Hard tiers. Since we use the left hand, targets moving right or up are kinematically favorable (“Easy”). Conversely, the Hard tier involves targets moving away or into occlusion zones, requiring complex reach-around maneuvers.

2) *Data Collection*: For the dynamic task, we collect a fine-tuning dataset of 2,000 successful episodes using a paused-sim oracle strategy. This oracle operates by pausing the physics simulation at every time step ( $N = 1$ ) to run the full VLA inference, thereby generating ideal closed-loop trajectories that perfectly track environmental changes—a behavior achievable only when computational latency is ignored. This automated pipeline allows for the scalable generation of high-quality expert data, avoiding the prohibitive time and labor costs associated with human VR teleoperation.

3) *Baselines and Configuration*: We use GR00T-N1.5-3B as the VLA backbone. We compare TIDAL against a standard Open-Loop Baseline under a strict Backbone-Iso-Compute protocol:

- Open-Loop Baseline: Follows the batch-and-execute paradigm. It queries the VLM backbone and Diffusion Head once at  $t = 0$ , generating a full action chunk ( $H = 16$ ), then executes the sequence open-loop ( $\sim 2.4$  Hz control frequency).
- TIDAL (Ours): Splits the compute budget. It queries the VLM once every 16 steps to cache the intent. Then, at every chunk of  $N = 4$  steps, it queries the flow matching head for a single Euler integration step, updating the action chunk based on the latest observation.

4) *Computational Protocols & Baseline Selection*: We strictly control the budget of the heavy Backbone components (VLM encoder and Diffusion Transformer). We fix the prediction horizon at  $H = 16$  for all methods. Reducing the horizon (e.g., to  $H = 8$ ) would require doubling the backbone query frequency to maintain continuous control. Given the latency of 3B models, such high-frequency re-planning is intractable for real-time deployment and would cause severe execution freezing.

We therefore enforce a backbone-iso-compute constraint. Both TIDAL and the baseline are limited to one VLM pass and an equivalent number of DiT passes per macrocycle. The distinction is topological, which is the baseline batches computations at  $t = 0$ , whereas TIDAL distributes

TABLE I  
SUCCESS RATE COMPARISON ON STATIC AND DYNAMIC BENCHMARKS

Method	Static (Official)	Dynamic (Easy)	Dynamic (Hard)
Baseline	<b>0.5925</b>	0.31	0.16
<b>TIDAL (Ours)</b>	0.5094	<b>0.61</b>	<b>0.36</b>

them temporally. While TIDAL incurs marginal overhead from lightweight MLP adapters(state encoding/action encoding and decoding) and the tiny custom 7-layer CNN motion predictor, these are negligible compared to the backbone latency. This ensures that performance gains come from hierarchical scheduling rather than increased backbone throughput.

We quantify latency using the performance of NVIDIA Jetson AGX Orin (Max-N mode, TensorRT from official performance profiles [1]). We define Effective Update Frequency based on total cycle time  $T_{cycle} = T_{inference} + T_{execution}$ , assuming a 50 Hz control rate (20ms/step):

- Baseline: Full inference (93 ms) + 16-step execution (320 ms)  $\rightarrow \sim 2.4$  Hz update rate.
- TIDAL (Effective): Weighted average inference ( $\sim 30$  ms, including amortized VLM) + 4-step execution (80 ms)  $\rightarrow \sim 9$  Hz effective update rate.
- TIDAL (Peak): Micro inference ( $\sim 19$  ms) + execution (80 ms)  $\rightarrow \sim 10$  Hz peak rate.

### B. Main Results

Table I summarizes the performance across standard static tasks and our dynamic interception benchmarks.

1) *Dynamic Interception*: In dynamic environments, the Open-Loop Baseline fails, scoring only 0.31 on the Easy tier and dropping to 0.16 on Hard. Its long inference latency prevents action chunk updates once execution begins. TIDAL doubles performance, reaching 0.61 (Easy) and 0.36 (Hard). This gap confirms our hypothesis: high-frequency correction is a prerequisite for interception, regardless of the semantic planner’s quality.

2) *Static Generalization*: On the official RoboCasa benchmark, the Baseline outperforms TIDAL (59.25% vs 50.94%). This gap comes from two factors. First, the VLM backbone was pre-trained with standard open-loop objectives, giving the Baseline an architectural advantage in static settings. Second, TIDAL’s hierarchical structure increases optimization complexity, likely requiring more training steps to converge. However, TIDAL retains strong generalist capabilities ( $\sim 50.94\%$ ), showing that optimizing inference for speed does not cause a severe loss of reasoning. We explicitly trade static precision for reactivity—a critical capability that baseline lacks.

### C. Ablation Study

We isolate the contributions of TIDAL’s two core components: hierarchical architecture (high-frequency updates) and differential motion Predictor (velocity perception). Table II shows results on the Dynamic (Easy) task.

The TIDAL architecture without motion features yields a success rate of 0.33, marginally better than the Baseline (0.31). Although operating at  $\sim 9$  Hz, it lacks explicit velocity data.

TABLE II  
ABLATION ANALYSIS ON DYNAMIC (EASY) TASKS.

Configuration	Success	Key Limitation
Baseline	0.31	High Latency + Static Features
TIDAL w/o Motion	0.33	Motion Blindness
Base + Motion	0.44	Execution Blind Spot
<b>TIDAL (Full)</b>	<b>0.61</b>	-

TABLE III  
HYPERPARAMETER EXPLORATION: HORIZON WEIGHT ( $w$ ) AND TIME SAMPLING ( $\alpha$ )

Weight	Loss Weight ( $w$ )	Time Sampling ( $\alpha$ )	
		Success Rate	Alpha
1.0	70.31%	3.0	78.12%
1.5	73.83%	<b>5.0</b>	<b>78.91%</b>
<b>2.0</b>	<b>76.95%</b>	7.0	71.10%
2.5	71.48%	-	-
3.0	70.70%	-	-

The policy acts as a high-frequency position servo that lags behind the moving target, confirming that control frequency is insufficient if perception remains motion-blind.

Injecting motion features into the Open-Loop Baseline improves performance to 0.44. Motion embeddings provide initial velocity cues, allowing the planner to estimate a better intercept trajectory at  $t = 0$ . However, this setup remains bound by the batch-and-execute paradigm; it cannot react to target changes during the long execution window.

TIDAL (Full) achieves 0.61, outperforming both variants. This highlights a critical synergy: the motion predictor provides the signal to track dynamics, while the hierarchical architecture provides the computational opportunity to act on that signal reactively.

#### D. Hyperparameter Exploration

We analyze TIDAL’s training objective sensitivity on a single representative task from the official suite, focusing on the horizon-weighting factor  $w$  (biasing the loss towards the immediate execution chunk) and the Beta distribution parameter  $\alpha$  (biasing time sampling towards the noise source).

We sweep  $w \in [1.0, 3.0]$  with  $\alpha = 1.5$ . Table III (Left) shows performance peaks at  $w = 2.0$  (76.95%). Increasing  $w$  to 2.0 improves success, confirming that prioritizing the first  $N = 4$  steps is crucial for micro-loop stability. Higher weights ( $w > 2.0$ ) degrade performance. Over-weighting likely causes the optimization to neglect trajectory continuity, creating disjointed flow predictions at chunk boundaries.

With  $w = 2.0$ , we vary  $\alpha$ . Since TIDAL’s micro-loop queries the flow network only from pure noise ( $t = 0$ ), the training distribution should match this pattern. Table III (Right) validates this. Increasing  $\alpha$  to 5.0 shifts focus towards  $t \approx 0$ , yielding the highest success rate (78.91%). This confirms that for single-step architectures, the capacity spent modeling mid-trajectory flow (e.g.,  $t \in [0.2, 0.8]$ ) is largely wasted. However, pushing  $\alpha$  too far (e.g., 7.0) reduces sample diversity, causing a performance drop.

TABLE IV  
ANALYSIS OF SEMANTIC INTENT LIFESPAN ( $l$ ) AND PERFORMANCE RETENTION

Lag Parameter ( $l$ )	Effective Steps	Success Rate	Retention
28 (Standard)	16 steps	0.72	100%
32	20 steps	0.68	94.4%
36	24 steps	0.61	84.7%
40	28 steps	0.66	91.7%
44	32 steps	0.69	95.8%
48	36 steps	0.69	95.8%
52	40 steps	0.66	91.7%
56	44 steps	0.60	83.3%
60	48 steps	0.48	66.7%
64	52 steps	0.38	52.8%
68	56 steps	0.51	70.8%
72	60 steps	0.32	44.4%
80	68 steps	0.24	33.3%
100	88 steps	0.20	27.8%

TABLE V  
COMPARISON OF INFERENCE STABILITY: PAUSED VS. NON-PAUSED PROTOCOLS

Method	Paused	Non-Paused	Retention Rate
Baseline	0.31	0.09	~29%
<b>TIDAL (Ours)</b>	<b>0.61</b>	<b>0.30</b>	<b>~49%</b>

#### E. Semantic Intent Lifespan and Efficiency

We analyze the temporal validity of the cached semantic intent  $\mathcal{E}$  on a single static task from official suite. By artificially increasing the latency parameter  $l$ , we force the micro-loop to execute more physical steps before refreshing the semantic goal, testing the policy’s tolerance for staleness.

Table IV shows a stable profile. Extending intent lifespan from the standard  $l = 28$  (0.72) to  $l = 56$  (0.60) causes minimal degradation. This suggests that in TIDAL, there is a window where the semantic embedding remains valid if the policy receives real-time proprioceptive updates.

This finding challenges the native action chunk limit. While the GR0OT backbone is trained to predict a fixed 16-step chunk, TIDAL’s hierarchical architecture extends the useful horizon of a single intent query to  $\sim 44$  steps. The policy uses the old intent to condition new, locally correct flows. A sharp performance cliff appears at  $l = 64$  (0.38), indicating where the robot’s state diverges too far from the initial snapshot. Although variance increases at extreme latencies ( $l > 60$ ), the trend confirms that control authority degrades as semantic lag exceeds the physical correlation window.

#### F. Sim-to-Real Potential: Non-Paused Inference

Standard benchmarks pause physics during inference, cutting the delay between observation and actuation off. To approximate real-world deployment, we use a non-paused evaluation where the simulation advances target dynamics during policy computation.

Table V reveals a contrast:

- **Baseline Collapse:** The Open-Loop Baseline fails, dropping from 0.31 to 0.09. Suffering from a  $\sim 400$  ms blind window (93 ms compute + 320 ms execution), the target moves away from the planned trajectory before the robot

moves. A 9% success rate makes the system unusable for real-time dynamic interception.

- **TIDAL Resilience:** TIDAL sustains a success rate of 0.30. By shrinking the update cycle to  $\sim$ 100ms, TIDAL reduces the blind window by  $4\times$ . Although performance drops compared to the idealized paused setting (0.61), it retains nearly half its performance and remains  $3\times$  more effective than the baseline. This resilience comes from our distributed compute strategy: interleaving computation with actuation minimizes reaction delay and continuously corrects for drift, bridging the reality gap where standard baselines fail.

## V. CONCLUSION

We presented TIDAL, a framework designed to enable high-frequency control with large VLA models. By interleaving single-step flow generation with action execution, our approach achieves a 4x increase in update frequency on edge hardware while maintaining the same backbone computational budget. This significantly reduces the execution blind spot found in standard batch-and-execute baselines.

We rely on temporally misaligned training to compensate for stale semantics, while single-step flow integration minimizes latency. This results in a 2x performance gain on dynamic interception tasks. Our analysis reveals that updating the policy with real-time proprioception effectively extends the lifespan of cached semantic embeddings beyond their native horizon. Since TIDAL is backbone-agnostic, it remains orthogonal to system-level accelerations. The sustained performance under non-paused protocols suggests strong potential for future sim-to-real transfer. We are currently deploying TIDAL on physical robot hardware to further validate its robustness in real-world dynamic environments.

## REFERENCES

- [1] J. Björck, F. Castañeda, N. Cherniadev, X. Da, R. Ding, L. Fan, Y. Fang, D. Fox, F. Hu, S. Huang *et al.*, “Gr00t n1: An open foundation model for generalist humanoid robots,” *arXiv preprint arXiv:2503.14734*, 2025.
- [2] K. Black, N. Brown, D. Driess, A. Esmail, M. Equi, C. Finn, N. Fusai, L. Groom, K. Hausman, B. Ichter *et al.*, “ $\pi_0$ : A vision-language-action flow model for general robot control,” *arXiv preprint arXiv:2410.24164*, 2024.
- [3] K. Kawaharazuka, J. Oh, J. Yamada, I. Posner, and Y. Zhu, “Vision-language-action models for robotics: A review towards real-world applications,” *IEEE Access*, 2025.
- [4] R. Shao, W. Li, L. Zhang, R. Zhang, Z. Liu, R. Chen, and L. Nie, “Large vlm-based vision-language-action models for robotic manipulation: A survey,” *arXiv preprint arXiv:2508.13073*, 2025.
- [5] K. Black, M. Y. Galliker, and S. Levine, “Real-time execution of action chunking flow policies,” *arXiv preprint arXiv:2506.07339*, 2025.
- [6] J. Tang, Y. Sun, Y. Zhao, S. Yang, Y. Lin, Z. Zhang, J. Hou, Y. Lu, Z. Liu, and S. Han, “Vlash: Real-time vlas via future-state-aware asynchronous inference,” *arXiv preprint arXiv:2512.01031*, 2025.
- [7] H. Wang, C. Xiong, R. Wang, and X. Chen, “Bitvla: 1-bit vision-language-action models for robotics manipulation,” *arXiv preprint arXiv:2506.07530*, 2025.
- [8] X. Tan, Y. Yang, P. Ye, J. Zheng, B. Bai, X. Wang, J. Hao, and T. Chen, “Think twice, act once: Token-aware compression and action reuse for efficient inference in vision-language-action models,” *arXiv preprint arXiv:2505.21200*, 2025.
- [9] J. Wen, Y. Zhu, J. Li, M. Zhu, Z. Tang, K. Wu, Z. Xu, N. Liu, R. Cheng, C. Shen *et al.*, “Tinyvla: Towards fast, data-efficient vision-language-action models for robotic manipulation,” *IEEE Robotics and Automation Letters*, 2025.
- [10] H. Chen, J. Liu, C. Gu, Z. Liu, R. Zhang, X. Li, X. He, Y. Guo, C.-W. Fu, S. Zhang *et al.*, “Fast-in-slow: A dual-system foundation model unifying fast manipulation within slow reasoning,” *arXiv preprint arXiv:2506.01953*, 2025.
- [11] J. Liu, H. Chen, P. An, Z. Liu, R. Zhang, C. Gu, X. Li, Z. Guo, S. Chen, M. Liu *et al.*, “Hybridvla: Collaborative diffusion and autoregression in a unified vision-language-action model,” *arXiv preprint arXiv:2503.10631*, 2025.
- [12] B. Zitkovich, T. Yu, S. Xu, P. Xu, T. Xiao, F. Xia, J. Wu, P. Wohlhart, S. Welker, A. Wahid *et al.*, “Rt-2: Vision-language-action models transfer web knowledge to robotic control,” in *Conference on Robot Learning*. PMLR, 2023, pp. 2165–2183.
- [13] M. J. Kim, K. Pertsch, S. Karamcheti, T. Xiao, A. Balakrishna, S. Nair, R. Rafailov, E. Foster, G. Lam, P. Sanketi *et al.*, “Openvla: An open-source vision-language-action model,” *arXiv preprint arXiv:2406.09246*, 2024.
- [14] O. Mees, D. Ghosh, K. Pertsch, K. Black, H. R. Walke, S. Dasari, J. Hejna, T. Kreiman, C. Xu, J. Luo *et al.*, “Octo: An open-source generalist robot policy,” in *First Workshop on Vision-Language Models for Navigation and Manipulation at ICRA 2024*, 2024.
- [15] C. Chi, Z. Xu, S. Feng, E. Cousineau, Y. Du, B. Burchfiel, R. Tedrake, and S. Song, “Diffusion policy: Visuomotor policy learning via action diffusion,” *The International Journal of Robotics Research*, vol. 44, no. 10–11, pp. 1684–1704, 2025.
- [16] K. Black, N. Brown, J. Darpinian, K. Dhabalia, D. Driess, A. Esmail, M. R. Equi, C. Finn, N. Fusai, M. Y. Galliker *et al.*, “ $\pi_{0.5}$ : A vision-language-action model with open-world generalization,” in *9th Annual Conference on Robot Learning*, 2025.
- [17] Z. Fu, T. Z. Zhao, and C. Finn, “Mobile aloha: Learning bimanual mobile manipulation using low-cost whole-body teleoperation,” in *8th Annual Conference on Robot Learning*, 2024.
- [18] M. Shukor, D. Aubakirova, F. Capuano, P. Kooijmans, S. Palma, A. Zouitine, M. Aractingi, C. Pascal, M. Russi, A. Marafioti *et al.*, “Smolvla: A vision-language-action model for affordable and efficient robotics,” *arXiv preprint arXiv:2506.01844*, 2025.
- [19] J. Liu, M. Liu, Z. Wang, L. Lee, K. Zhou, P. An, S. Yang, R. Zhang, Y. Guo, and S. Zhang, “Robomamba: Multimodal state space model for efficient robot reasoning and manipulation,” *arXiv e-prints*, pp. arXiv–2406, 2024.
- [20] A. Prasad, K. Lin, J. Wu, L. Zhou, and J. Bohg, “Consistency policy: Accelerated visuomotor policies via consistency distillation,” *arXiv preprint arXiv:2405.07503*, 2024.
- [21] J. Lin, J. Tang, H. Tang, S. Yang, G. Xiao, and S. Han, “Awq: Activation-aware weight quantization for on-device llm compression and acceleration,” *GetMobile: Mobile Computing and Communications*, vol. 28, no. 4, pp. 12–17, 2025.
- [22] Y. Yang, Y. Wang, Z. Wen, L. Zhongwei, C. Zou, Z. Zhang, C. Wen, and L. Zhang, “Efficientvla: Training-free acceleration and compression for vision-language-action models,” *arXiv preprint arXiv:2506.10100*, 2025.
- [23] Y. Yue, Y. Wang, B. Kang, Y. Han, S. Wang, S. Song, J. Feng, and G. Huang, “Deer-vla: Dynamic inference of multimodal large language models for efficient robot execution,” *Advances in Neural Information Processing Systems*, vol. 37, pp. 56619–56643, 2024.
- [24] W. Song, J. Chen, P. Ding, Y. Huang, H. Zhao, D. Wang, and H. Li, “Ceed-vla: Consistency vision-language-action model with early-exit decoding,” *arXiv preprint arXiv:2506.13725*, 2025.
- [25] R. Zhang, M. Dong, Y. Zhang, L. Heng, X. Chi, G. Dai, L. Du, Y. Du, and S. Zhang, “Mole-vla: Dynamic layer-skipping vision language action model via mixture-of-layers for efficient robot manipulation,” *arXiv preprint arXiv:2503.20384*, 2025.
- [26] P. Budzianowski, W. Maa, M. Freed, J. Mo, W. Hsiao, A. Xie, T. Mloduchowski, V. Tipnis, and B. Bolte, “Edgevla: Efficient vision-language-action models,” *arXiv preprint arXiv:2507.14049*, 2025.
- [27] W. Song, J. Chen, P. Ding, H. Zhao, W. Zhao, Z. Zhong, Z. Ge, J. Ma, and H. Li, “Accelerating vision-language-action model integrated with action chunking via parallel decoding,” *arXiv preprint arXiv:2503.02310*, 2025.
- [28] Y. Ma, Y. Zhou, Y. Yang, T. Wang, and H. Fan, “Running vlas at real-time speed,” *arXiv preprint arXiv:2510.26742*, 2025.
- [29] S. Wang, R. Yu, Z. Yuan, C. Yu, F. Gao, Y. Wang, and D. F. Wong, “Spec-vla: speculative decoding for vision-language-action models with relaxed acceptance,” in *Proceedings of the 2025 Conference on Empirical Methods in Natural Language Processing*, 2025, pp. 26916–26928.

- [30] T. Zou, H. Zeng, Y. Nong, Y. Li, K. Liu, H. Yang, X. Ling, X. Li, and L. Ma, “Asynchronous fast-slow vision-language-action policies for whole-body robotic manipulation,” *arXiv preprint arXiv:2512.20188*, 2025.
- [31] W. Guan, Q. Hu, A. Li, and J. Cheng, “Efficient vision-language-action models for embodied manipulation: A systematic survey,” *arXiv preprint arXiv:2510.17111*, 2025.
- [32] S. Xu, Y. Wang, C. Xia, D. Zhu, T. Huang, and C. Xu, “Vla-cache: Towards efficient vision-language-action model via adaptive token caching in robotic manipulation,” *arXiv preprint arXiv:2502.02175*, 2025.
- [33] Z. Duan, Y. Zhang, S. Geng, G. Liu, J. Boedecker, and C. X. Lu, “Fast ecot: Efficient embodied chain-of-thought via thoughts reuse,” *arXiv preprint arXiv:2506.07639*, 2025.
- [34] T. Z. Zhao, V. Kumar, S. Levine, and C. Finn, “Learning fine-grained bimanual manipulation with low-cost hardware,” *arXiv preprint arXiv:2304.13705*, 2023.
- [35] R. Xu, J. Zhang, M. Guo, Y. Wen, H. Yang, M. Lin, J. Huang, Z. Li, K. Zhang, L. Wang *et al.*, “A0: An affordance-aware hierarchical model for general robotic manipulation,” *arXiv preprint arXiv:2504.12636*, 2025.
- [36] K. Black, A. Z. Ren, M. Equi, and S. Levine, “Training-time action conditioning for efficient real-time chunking,” *arXiv preprint arXiv:2512.05964*, 2025.
- [37] Y. Liu, J. I. Hamid, A. Xie, Y. Lee, M. Du, and C. Finn, “Bidirectional decoding: Improving action chunking via closed-loop resampling,” *arXiv preprint arXiv:2408.17355*, 2024.
- [38] X. Liu, C. Gong, and Q. Liu, “Flow straight and fast: Learning to generate and transfer data with rectified flow,” *arXiv preprint arXiv:2209.03003*, 2022.
- [39] S. Jiang, X. Fang, N. Roy, T. Lozano-Pérez, L. P. Kaelbling, and S. Anch, “Streaming flow policy: Simplifying diffusion / flow-matching policies by treating action trajectories as flow trajectories,” *arXiv preprint arXiv:2505.21851*, 2025.
- [40] S. H. Høeg, Y. Du, and O. Egeland, “Streaming diffusion policy: Fast policy synthesis with variable noise diffusion models,” *arXiv preprint arXiv:2406.04806*, 2024.
- [41] Y. Lipman, R. T. Chen, H. Ben-Hamu, M. Nickel, and M. Le, “Flow matching for generative modeling,” *arXiv preprint arXiv:2210.02747*, 2022.
- [42] S. Nasiriany, A. Maddukuri, L. Zhang, A. Parikh, A. Lo, A. Joshi, A. Mandlekar, and Y. Zhu, “Robocasa: Large-scale simulation of everyday tasks for generalist robots,” *arXiv preprint arXiv:2406.02523*, 2024.